ARTICLE

Influence of interpenetration on the flexibility of MUV-2

María Vicent-Morales,[a] Iñigo J. Vitórica-Yrezábal,[b] Manuel Souto*[a] and Guillermo Mínguez Espallargas*[a]

The crystal structure of an interpenetrated tetrathiafulvalene(TTF)-based metal-organic framework (MOF) is reported. This MOF, denoted **MUV-2-i**, is the interpenetrated analogue of the hierarchical and flexible MUV-2. Interestingly, the large flexibility exhibited by **MUV-2** upon polar solvent adsorption is considerably reduced in the interpenetrated form which can be explained by short S···S interactions between adjacent TTF-based ligands ensuring more rigidity to the framework. In addition, porosity of **MUV-2-i** significantly decreased in comparison to **MUV-2** as shown by the reduced free volume in the crystal structure.

Introduction

Metal-organic frameworks (MOFs) or porous coordination polymers (PCPs) are a class of porous crystalline hybrid materials constructed from metal ions or clusters and organic ligands via coordination bonds. Research on MOFs has gathered increased interest because of their structural and functional tunability as well as their high potential applications in gas storage, separation, and catalysis, among others.[1–3]

Flexible or "breathing" MOFs are very interesting materials since they can exhibit large changes in their cell volumes upon external stimuli such as guest inclusion, temperature or pressure.[4,5] For example, MIL-53[6], MIL-88[7], SHF-61[8] and some soft porous crystals reported by Kitagawa[9] are materials which can exhibit structural changes upon exposure to external stimuli with defined phase transitions or driven by a continuous breathing process. We have recently reported a highly stable tetrathiafulvalene(TTF)-based MOF, namely **MUV-2** (MUV: Materials of University of Valencia), which shows a hierarchical structure with both mesoporous and orthogonal microporous channels.[10] Moreover, this MOF exhibits a reversible swelling behaviour (up to 40% of the volume cell) upon polar solvent adsorption which directly impacts on the planarity of the flexible TTF linkers modifying its oxidation potential.[11] Hence, this material could be very promising to develop new electrochemical sensors.

One limitation of porous materials is interpenetration, also referred as catenation, a common phenomenon observed in MOFs, especially those presenting large pores, where one or more frameworks can grow occupying the void space in order to stabilize the resulting structure which can modify, for example, the morphology, porosity and other functional properties.[12,13] Although interpenetration is typically considered as an undesired result, it is sometimes accompanied with great benefits, such as improved gas separation capacity.[14] However, controlling interpenetration to synthesise a crystalline material with a desired porosity and functionalities is still a challenge since it depends on multiple synthetic parameters such temperature, concentration,[15] modulator,[16] pH,[17,18] and ligand design.[19,20] In addition, partially interpenetrated MOFs can be achieved controlling such parameters with a mixture of interpenetrated and non-interpenetrated components.[21,22]

In a flexible MOF, tuning the breathing behaviour through interpenetration is a very interesting phenomenon in order to modulate and control some of their functional, but this has been scarcely investigated.[23] For example, Serre and co-workers reported the interpenetrated version of MIL-88, denoted as MIL-126, which shows a rigid structure and permanent porosity in contrast to its non-interpenetrated analogue which exhibits large flexibility.[24] The rigidity of MIL-126 was attributed to the presence of strong $\pi-\pi$ interactions between adjacent phenyl rings and hydrogen bond contacts which prevented the structure from any shrinkage.

Herein we present the crystal structure of **MUV-2-i(pyridine)**, of formula (TTFTB)$_3$[(Fe$_3$O)(py)$_3$]$_2$·0.36py (H$_4$TTFTB = tetrathiafulvalene tetrabenzoic acid; py = pyridine), which shows an interpenetrated framework and a remarkable decrease of free volume in comparison to the non-interpenetrated **MUV-2**. Interestingly, **MUV-2-i** shows more rigidity when soaking the material with polar solvents such as pyridine or DMF, in contrast to **MUV-2,** which has been demonstrated to "breathe" upon immersion on these solvents.[11]
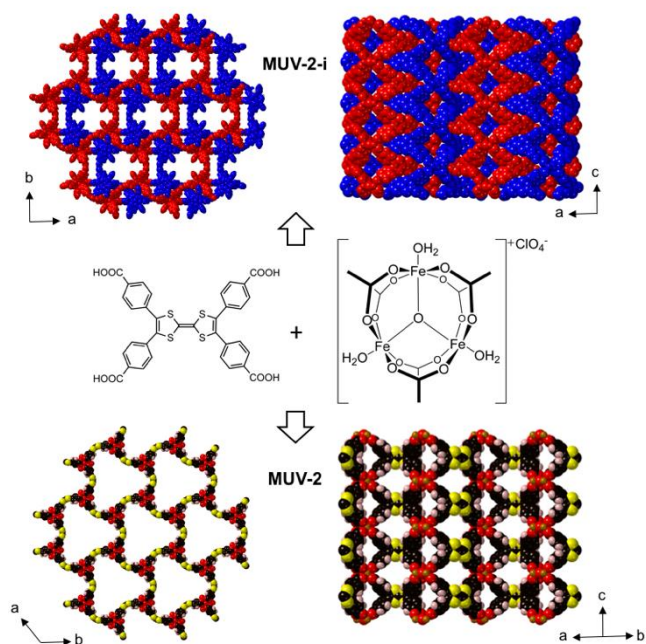
Figure 1. Chemical structures of the ligand and of the [Fe₃O(CH₃COO)₆]ClO₄ secondary building unit used in the synthesis of **MUV-2-i** and **MUV-2**. Schematic representation of the crystal structures of **MUV-2-i** (the two interpenetrating nets coloured in red and blue) and **MUV-2** along the *c*-axis and perpendicular view of the structure. Black, yellow, red, orange and pink balls represent C, S, O, Fe and H, respectively.

Results and discussion

Synthesis of MUV-2-i

MUV-2-i was synthesised by reacting the preformed cluster [Fe₃O(CH₃COO)₆]ClO₄[10] (0.02 mmol), tetrathiafulvalene tetrabenzoic acid (H₄TTFTB) (0.03 mmol) with acetic acid (1 mL) in 4 mL of *N,N*-dimethylformamide (DMF) at 105°C for 48 hours. The crystals were washed with large amount of DMF in order to remove any unreacted starting material, immersed with EtOH at 65°C for 2h, filtered and dried at 150°C in the oven for 2h, yielding the dried material denoted **MUV-2-i(dry)**. These dark red crystals were soaked in pyridine resulting in **MUV-2-i(pyridine)**, which were used to determine the crystal structure by single-crystal X-ray diffraction. It is important to note that we performed an exhaustive study on the synthetic methodology to control the synthesis of **MUV-2-i** modifying different parameters (temperature, concentration, solvents, pH) obtaining the non-interpenetrated **MUV-2** crystal structure most times as checked by powder X-ray diffraction (PXRD) (see Supporting Information). We speculated about the possibility that the ligand used in the synthesis of MUV-2-i contained some traces of HCl or water as deduced from the NMR spectrum (Figure S1). In order to study the effect of water concentration on the formation of **MUV-2-i**, we have added small amounts of water to the synthesis reaction (Figure S4) observing in most cases the formation of **MUV-2** whereas the presence of a mixture of phases were observed when adding large amount of water. However, we were not able to totally control the reproducibility of the synthesis of **MUV-2-i** which was obtained only in few cases by serendipity.
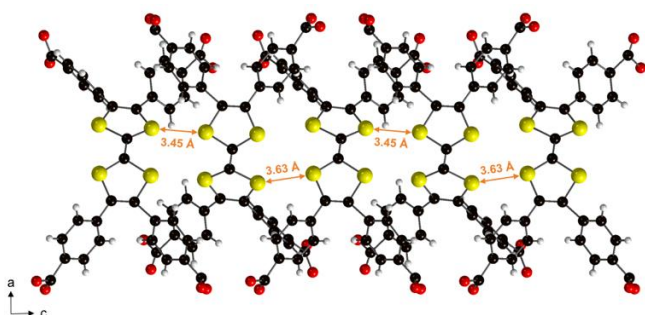
Crystal structure of MUV-2-i

Table 1. Crystal data and structure refinement for **MUV-2-i**.

Empirical formula	C₇₂.₇₉H₄₅.₇₉Fe₃N₄.₃₆O₁₃S₆
Formula weight	1549.35
Temperature/K	100.0
Crystal system	orthorhombic
Space group	$C222_1$
a /Å	34.2069(7)
b /Å	57.0341(9)
c /Å	12.1673(2)
α /°	90
β /°	90
γ /°	90
Volume /Å³	23737.9(7)
Z	8
ρ_calc /g·cm⁻³	0.867
μ /mm⁻¹	0.461
F(000)	6328.0
Crystal size /mm³	0.04 × 0.02 × 0.02
Radiation	(λ = 0.6889)
2Θ range for data collection /°	3.512 to 49.038
Index ranges	-41 ≤ h ≤ 41, -68 ≤ k ≤ 68, -14 ≤ l ≤ 14
Reflections collected	141606
Independent reflections	21742 [R_int = 0.1330, R_sigma = 0.0744]
Data / restraints / parameters	21742 / 2130 / 1114
Goodness-of-fit on F²	1.370
Final R indexes [I>=2σ (I)]	R₁ = 0.1143, wR₂ = 0.3166
Final R indexes [all data]	R₁ = 0.1221, wR₂ = 0.3262
Largest diff. peak/hole / e Å⁻³	1.63/-1.18
Flack parameter	0.49(4)

The crystal structure of **MUV-2-i(pyridine)** was determined by single-crystal X-ray diffraction measured up to 0.8 Å resolution at the I19 beamline facilities at Diamond Light Source (UK), which is a better resolution than the one observed for the non-interpenetrated **MUV-2**, in agreement with a better diffraction of a less porous system. **MUV-2-i(pyridine)**

crystallises in the orthorhombic system (space group $C222_1$) (Table 1), in contrast to **MUV-2** (hexagonal, space group P-62m). The unit cell parameters of **MUV-2-i(pyridine)** are a = 34.2 Å; b = 57.0 Å; c = 12.2 Å (V = 23737 Å^3) and, on the basis of the tetratopic TTFTB ligands and six-connected $Fe_3O(COO)_6$ nodes, **MUV-2-i** can be described as a 3,6-connected network with *ttp* topology (Figure 1), which is the same than for **MUV-2**.[11] Crystal structure of **MUV-2-i** shows an interwoven network revealing microporous channels of *ca.* 9x10 Å, in contrast to the large hexagonal mesopores of *ca.* 3.3 nm exhibited by **MUV-2** in the crystalline phase in which the TTF ligands have a similar degree of bending (**MUV-2(31)**).[11]

On the other hand, partial view of the **MUV-2-i** structure along *b*-axis reveals S···S short contacts of 3.45 and 3.6 Å between adjacent TTFTB ligands forming a kind of herringbone stacks (Figure 2) whereas in the non-interpenetrated structure of **MUV-2** the S···S distances between adjacent TTFTB ligands along the same axis are considerably larger (9.4 Å). Interestingly, the TTFTB molecules in **MUV-2-i** are significantly distorted with calculated dihedral angles (θ) formed by the two dithiole rings (planes S1-C1-C2-S2 and S3-C5-C6-S4) of 36° and 73°, which are much higher than in the case of non-interpenetrated **MUV-2** when is also solvated with pyridine (9°). It is important to note that since crystals were immersed in pyridine in both cases, crystal structure shows that three molecules of pyridine are coordinated to $Fe_3O(COO)_6$ nodes instead of water molecules, as it was also observed for **MUV-2**.[11] Finally, the calculated free space of **MUV-2-i** is 55 % which is significantly lower than the non-interpenetrated **MUV-2** (82 %) in agreement with BET calculations from N_2 adsorptions (BET values of 410 and 1220 m^2/g, respectively) (Figure 3).


Figure 2. Partial view along *b*-axis of the crystal structure of **MUV-2-i** showing the distances (3.45 and 3.64 Å) of lateral S···S interactions between the TTFTB moieties.

Flexibility of MUV-2-i

In addition to the expected decrease of free volume caused by interpenetration, we observe a significant quenching of the breathing phenomena characteristic of **MUV-2**.[11] Thus, upon immersion to a solvent that opens the structure in **MUV-2** (e.g. pyridine or DMF), the powder X-ray diffraction (PXRD) pattern of **MUV-2-i** reveals that the principal peak is slightly shifted from 2θ = 3.4° (d = 25.96 Å) in the desolvated form to 2θ = 3.1° (d = 28.48 Å) as shown in Figure 4, in agreement with the

simulated pattern from the crystal structure (Figure S3). However, under the same conditions, the principal peak of the non-interpenetrated **MUV-2** is shifted to 2θ = 2.9° (d = 30.44 Å) upon soaking the MOF in pyridine or DMF, with a larger pore aperture and a pore diameter of 3.5 nm (Figure 5). This allows an easy and fast differentiation between the two structures, otherwise difficult to be achieved. Indeed, we were able to identify a mixture of phases in some cases where the appearance of both peaks (2.9° and 3.1°) indicates the presence of a mixture of **MUV-2** and **MUV-2-i** (Figure S4).
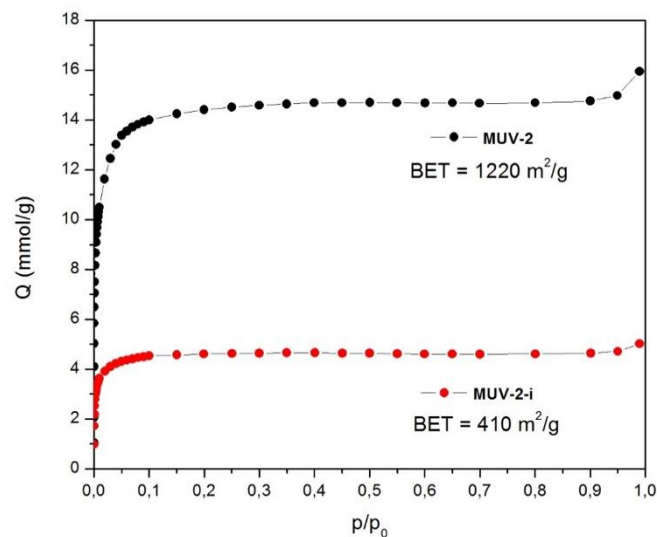
Figure 3. Nitrogen adsorption isotherms at 77 K on **MUV-2** (black) and **MUV-2-i** (red).
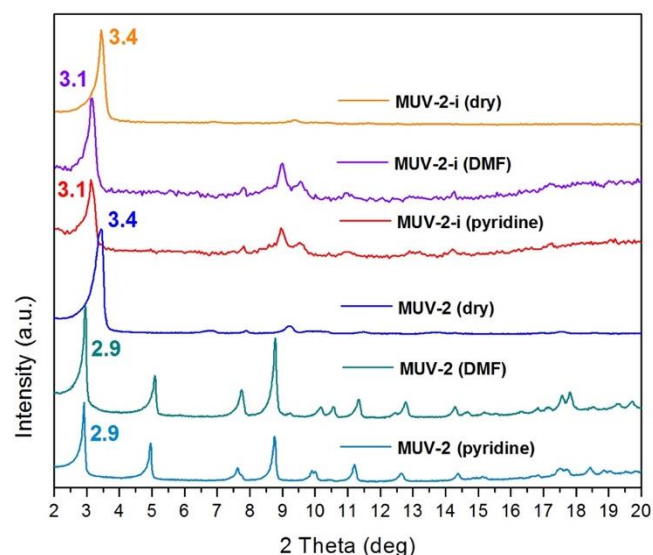
Figure 4. PXRD patterns for **MUV-2-i** and **MUV-2** (dried) and after soaking with pyridine and DMF at room temperature.

Cell parameters were obtained from the PXRD patterns for **MUV-2-i** and **MUV-2** dried, soaked in DMF and soaked in pyridine, in order to compare the different breathing amplitudes (Table 1). The changes in the cell volume between the dried forms and the solvated forms is around 20% for **MUV-2-i**, which is the half of the breathing amplitude for **MUV-2** (*ca.*

40%) under the same conditions. These values indicate that interpenetrated **MUV-2-i** presents a smaller breathing behaviour upon solvent adsorption in addition to the reduced nitrogen sorption capacity. These results differ from those for MIL-88 and MIL-126; whereas MIL-88 exhibits a large breathing behaviour upon solvent adsorption (230% breathing amplitude) but no nitrogen adsorption, MIL-126 shows negligible breathing (2% breathing amplitude) but a larger nitrogen sorption capacity.[24] In our case, **MUV-2-i** shows an intermediate degree of flexibility while maintaining the permanent porosity at the same time.

Table 1. Cell parameters and breathing amplitude (%) of the dried and solvated forms with pyridine and/or DMF for MUV-2, MUV-2-i, MIL-88 and MIL-126. BET surface areas of MUV-2, MUV-2-i, MIL-88 and MIL-126.

	a (Å)	c (Å)	Volume (Å^3)	Breathing amplitude (%)[c]	BET surface area (m^2/g)[d]
MUV-2 (dry)	29.5	12.5	9375	–	
MUV-2 (pyridine)	35.8	12.3	13710	46	1220
MUV-2 (DMF)	34.9	12.4	13067	39	
MUV-2-i (dry) [a]	29.2	12.3	9051	–	
MUV-2-i (pyridine) [a]	31.8	12.4	10846	20	410
MUV-2-I (DMF) [a]	31.7	12.4	10760	19	
MIL-88 (dry) [b]	10.2	27.6	2490	–	
MIL-88D (pyridine) [b]	20.5	22.1	8200	230	N.A.
MIL-126 (dry) [b]	21.5	35.8	16525	–	
MIL-126 (DMF) [b]	21.7	35.6	16780	2	1750

[a] Refinement performed using the hexagonal cell analogous to MUV-2 for ease of comparison. [b] Values obtained from ref. 24. [c] Amplitude = ($V_{max} - V_{min}/V_{min}$)*100. [d] Measured with N$_2$ at 77 K.
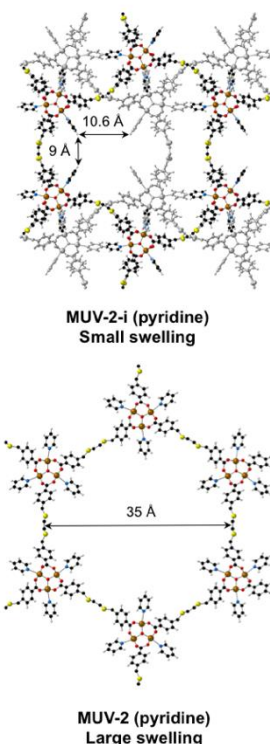
Figure 5. Representation of the pores with distances in the crystal structure of **MUV-2-i** and **MUV-2** when soaking them with pyridine at room temperature. **MUV-2-i** exhibits a smaller breathing phenomenon than **MUV-2**.

The weaker breathing behaviour, i.e. smaller pore aperture, which is taking place in the interpenetrated **MUV-2-i** structure can be explained in terms of intermolecular interactions between the TTFTB moieties. Whereas in the non-interpenetrated structure the TTFTB ligands are considerably far with S···S distances of 9.4 Å between adjacent ligands along the *b*-axis, the interpenetrated **MUV-2-i** structure reveals S···S short contacts of 3.45 Å (Figure 2) which could be responsible for the largest rigidity of the framework.

Conclusions

In summary, we have reported the interpenetrated structure **MUV-2-i**, an analogue MOF of the flexible and hierarchical **MUV-2**, albeit exhibiting reduced free volume and decreased pore sizes. In addition, the structure becomes more rigid than the non-interpenetrated **MUV-2** structure when the MOF is solvated with polar solvents probably due to short S···S interactions between the TTFTB ligands. We believe that this study will be useful for the scientific community to distinguish between interpenetrated/non-interpenetrated structures and to further understand how to fully control the synthesis and properties of each structure.

Conflicts of interest

There are no conflicts to declare.

Acknowledgements

Notes and references

1   H. Furukawa, K. E. Cordova, M. O'Keeffe and O. M. Yaghi, *Science*, 2013, **341**, 1230444.

2   H.-C. Zhou and S. Kitagawa, *Chem. Soc. Rev.*, 2014, **43**, 5415–5418.

3   G. Maurin, C. Serre, A. Cooper and G. Férey, *Chem. Soc. Rev.*, 2017, **46**, 3104–3107.

4   A. Schneemann, V. Bon, I. Schwedler, I. Senkovska, S. Kaskel and R. A. Fischer, *Chem. Soc. Rev.*, 2014, **43**, 6062–6096.

5   R. E. Morris and L. Brammer, *Chem. Soc. Rev.*, 2017, **46**, 5444–5462.

6   C. Serre, F. Millange, C. Thouvenot, M. Noguès, G. Marsolier, D. Louër and G. Férey, *J. Am. Chem. Soc.*, 2002, **124**, 13519–13526.

7   G. Férey, C. Mellot-Draznieks, C. Serre, F. Millange, J. Dutour, S. Surblé and I. Margiolaki, *Science*, 2005, **309**, 2040–2042.

8   E. J. Carrington, C. A. McAnally, A. J. Fletcher, S. P. Thompson, M. Warren and L. Brammer, *Nat. Chem.*, 2017, **9**, 882–889.

9   H. Sato, W. Kosaka, R. Matsuda, A. Hori, Y. Hijikata, R. V Belosludov, S. Sakaki, M. Takata and S. Kitagawa, *Science*, 2014, **343**, 167–170.

10   M. Souto, A. Santiago-Portillo, M. Palomino, I. Vitorica-Yrzebal, B. J. C. Vieira, J. C. C. Waerenborgh, S. Valencia, S. Navalon, F. Rey, H. Garcia and G. Minguez Espallargas, *Chem. Sci.*, 2018, **9**, 2413–2418.

11   M. Souto, J. Romero, J. Calbo, I. J. Vitorica-Yrezabal, J. L. Zafra, J. Casado Cordón, E. Ortí, A. Walsh and G. Minguez Espallargas, *J. Am. Chem. Soc.*, 2018, **140**, 10562–10569.

12   H. L. Jiang, T. A. Makal and H. C. Zhou, *Coord. Chem. Rev.*, 2013, **257**, 2232–2249.

13   Y. N. Gong, D. C. Zhong and T. B. Lu, *CrystEngComm*, 2016, **18**, 2596–2606.

14   P. Nugent, Y. Belmabkhout, S. D. Burd, A. J. Carins, R. Luebke, K. Forrest, T. Pham, S. Ma, B. Space, L. Wojtas, M. Eddaoudi and M. J. Zaworotko, *Nature*, 2013, **495**, 80–84.

15   J. J. Zhang, L. Wojtas, R. W. Larsen, M. Eddaoudi and M. J. Zaworotko, *J. Am. Chem. Soc.*, 2009, **131**, 17040–17041.

16   J. Duan, J. Bai, B. Zheng, Y. Li and W. Ren, *Chem. Commun.*, 2011, 2556–2558.

17   K. P. Rao, M. Higuchi, J. Duan and S. Kitagawa, *Cryst. Growth Des.*, 2013, **13**, 981–985.

18   S. Surinwong, N. Yoshinari, T. Kojima and T. Konno, *Chem. Commun.*, 2016, **52**, 12893–12896.

19   O. K. Farha, C. D. Malliakas, M. G. Kanatzidis and J. T. Hupp, *J. Am. Chem. Soc.*, 2010, **132**, 950–952.

20   R. J. Marshall, C. T. Lennon, A. Tao, H. M. Senn, C. Wilson, D. Fairen-Jimenez and R. S. Forgan, *J. Mater. Chem. A*, 2018, **6**, 1181–1187.

21   S. Yang, X. Lin, W. Lewis, M. Suyetin, E. Bichoutskaia, J. E. Parker, C. C. Tang, D. R. Allan, P. J. Rizkallah, P. Hubberstey, N. R. Champness, K. M. Thomas, A. J. Blake and M. Schröder, *Nat. Mater.*, 2012, **11**, 1–7.

22   D. O. Nolan, D. G. Madden, A. Kumar, K. Chen, T. Pham, K. A. Forrest, E. Patyk-kazmierczak, Q. Yang, C. A. Murray, C. C. Tang and M. J. Zaworotko, *Chem. Commun.*, 2018, **54**, 3488–3491.

23   J. H. Park, W. R. Lee, Y. Kim, H. J. Lee, D. W. Ryu and W. J. Phang, *Cryst. Growth Des.*, 2014, **14**, 699–704.

24   M. Dan-Hardi, H. Chevreau, T. Devic, P. Horcajada, G. Maurin, G. Férey, D. Popov, C. Riekel, S. Wuttke, J. C. Lavalley, A. Vimont, T. Boudewijns, D. De Vos and C. Serre, *Chem. Mater.*, 2012, **24**, 2486–2492.